Batteries & Supercaps

Research Article
doi.org/10.1002/batt.202500382

Chemistry Europe
European Chemical Societies Publishing

www.batteries-supercaps.org

Tailoring Adsorption Properties of Graphitic Surfaces: Toward Improved Anode Materials for Li- and Post-Li Ion Batteries

Jafar Azizi, Axel Groß, and Holger Euchner*

The adsorption of alkali metal (AM) atoms on graphitic surfaces is one of the processes that determine the performance of carbon-based anode materials. In particular, when graphite derivatives such as hard carbon with increased surface area are considered, adsorption accounts for a significant amount of the AM storage capacity. While it is well known that the adsorption of Li and Na on pristine graphite is energetically unfavorable, this article shows how graphitic surfaces can be modified to tailor their adsorption properties. For this purpose, the adsorption of Li, Na, and K on graphitic model systems, containing defects and impurities as well as combinations thereof, is investigated by means of density functional theory. The results show that particular defects and impurity atoms can modify the adsorption strength of the surface such that Li and Na adsorption become energetically favorable, while at the same time, capacity loss via trapping of AM atoms is minimized.

1. Introduction

Due to their high energy density and reliability, rechargeable lithium-ion batteries (LIBs) currently dominate the energy storage market.[1–4] However, the increasing demand has resulted in the quest for new battery technologies and brought attention to post-lithium ion systems.[5–8] Here, chemical similarity as well as abundance makes Na and K potential candidates to substitute Li. Yet, while graphite is the standard anode material for LIBs, research on Na-ion batteries (NIBs) has demonstrated that graphite is unsuited as an anode material for NIBs.[9,10] In fact, graphite provides an almost negligible capacity for the intercalation of Na, and with increasing concentration, Na intercalation becomes thermodynamically unstable.[11,12] K on the other hand, shows a similar behavior as Li. However, the maximum capacity for Li storage corresponds to a LiC_6 stoichiometry, whereas K intercalation compounds reach their concentration limit with a lower K content of KC_8.[13,14]

As a consequence, in particular for the case of Na, new anode materials for post-Li systems are needed, with rising interest in hard carbon (HC). HC is a carbon based material with a large degree of disorder that has the potential to effectively replace graphite.[15–19] With stable cycling and increased specific capacities that can surpass 300 mAh g^{-1}, HC is able to store reasonable amounts of Na.[20] Additionally, HC can be produced using precursors found in a wide range of low-cost biomass materials, including wood, peat moss, lignin, or banana leaves, thus satisfying the sustainability requirements of economic viability and environmental friendliness.[21–24]

From a synthesis point of view, it is interesting to note that precursors with high sp^2 hybridization, like aromatic petroleum derivatives, will typically rather form so-called soft carbon with a higher graphitic content after carbonization.[25–27] Precursors with high sp^3 carbon content, like cellulose and polymers, typically create more complex, disordered structures with small and strongly cross-linked graphitic domains. This results in a stiff structure with increased hardness that does not transform into graphite at high temperatures, therefore also referred to as non-graphitizable (hard) carbon. Moreover, HC shows high defect concentrations as well as differently sized voids, so-called micro- or nano-pores. Typically, two to five imperfect graphitic layers are stacked in graphitic domains, resulting in a wider interlayer spacing of 3.7–4.0 Å, which is an advantage for the alkali metal (AM) intercalation in HC anodes.[28] Depending on the synthesis conditions, the size and quantity distributions of micro- and nano-pores produced by this turbostatic network strongly differ. The presence of these micro- and nano-pores and their significant storage capacity makes the investigation of surfaces and surface-like parts important to gain further insights into the storage process. Furthermore, different types of vacancies, topological defects, or heteroatom contaminations can influence the local geometry, for instance, causing a bending of graphene sheets.[29–32] Defects and impurities can also significantly alter the properties of the material, changing, e.g., the mechanical

J. Azizi, A. Groß
Institute of Theoretical Chemistry
Ulm University
D-89081 Ulm, Germany

H. Euchner
Institute of Physical and Theoretical Chemistry
Tübingen University
72076 Tübingen, Germany
E-mail: holger.euchner@uni-tuebingen.de

Supporting information for this article is available on the WWW under https://doi.org/10.1002/batt.202500382

or electronic properties. For instance, it has been proposed that doping may boost the surface wettability, thus improving battery performance and AM storage capacity.[16,33–35]

In addition, it is well accepted that defect sites can accommodate Li, Na, and K atoms on hard carbon surfaces.[36–39] Li et al. have, for instance, demonstrated that increased defect concentrations result in significantly improved Na storage capacity of hard carbon.[16] Similarly, it was shown that the storage capacity in different regions of the charge/discharge curve as well as the structural stability can be modified by heteroatom doping.[40] While defects and impurities have been shown to be able to increase the specific capacity of carbonaceous materials, the higher reactivity of defect and doping sites can also result in irreversible capacity loss as AM atoms can be trapped and side reaction can be promoted. This means that defects and impurity atoms have the ability to alter energetics and kinetics of carbon based electrode materials, which can strongly affect the resulting battery performance. Hence, a detailed understanding of the storage process with respect to defects and impurities may allow tailoring improved anode materials.

In this context, computational studies have been utilized in conjunction with experimental research to provide a fundamental knowledge on the storage of Li, Na, and K in the graphitic bulk-like parts of HC, however, surfaces—as main constituents of micro- and nano-pores—containing defects and impurities are hardly investigated.[41–44] While we have studied the effect of defects in the intercalation of bulk graphite in our previous work,[45,46] we, here, extend these studies and consider the impact of defects and heteroatom impurities on the adsorption properties of graphitic surfaces. Our results show that surface modifications can indeed significantly alter the AM adsorption and may thus result in an improved AM storage capacity.

2. Computational Methods

To investigate the impact of different structural motives and impurities on the properties of hard carbon surfaces, simplified model systems have been studied by density functional theory. Different defect types such as mono-vacancy (MV), Stone–Wales (SW) defect, as well as the combination of MV and SW defects (MSW) have been investigated. Furthermore, adatom (AA) defects and a variety of impurities such as boron (B), nitrogen (N), sulfur (S), silicon (Si), and OH were considered. The resulting adsorption sites have been studied in a two-layer graphite system based on a $6 \times 6 \times 1$ unit cell. Due to the large lateral size of the considered systems, we have restricted ourselves to a two-layer model. This results in a slight underestimation of adsorption energies in the order of 50 meV (see Figure S1, Supporting Information).

All simulations were performed with the Vienna Ab Initio Simulation Package (VASP),[47] using the Projector Augmented Wave approach.[48] Exchange and correlation were described via the optPBE functional, which includes a non-local correction scheme to account for van der Waals interactions.[49] After optimization of the respective bulk systems, a large vacuum of almost 36 Å was introduced above the defect/impurity-containing layer to create the corresponding surface models (see Figure S2, Supporting Information). The electronic structure was optimized until the energy difference between the self-consistent field cycles fell below 10^{-7} eV, while the ionic geometry was relaxed until force differences of less than 10^{-3} eV Å^{-1} were reached. Each structure was optimized with respect to lattice constant and atomic positions, leaving the top layer free to move, whereas the bottom layer was kept fixed. While the underlying bulk structures were optimized with a $4 \times 4 \times 4$ k-point mesh, the considered surface models were optimized using a $4 \times 4 \times 1$ k-point mesh, applying a plane wave cutoff of 600 eV.

In addition, the nudged elastic band (NEB) method[50,51] with five images along the reaction path was applied to evaluate the minimum energy path for AM migration for a few selected systems.

Finally, to describe the AM adsorption on edge sites, a three-layer graphite system, again based on a 6×6 unit cell was considered. Here, a large vacuum of 36 Å was applied in all directions of the supercell and a $1 \times 1 \times 1$ k-point mesh was utilized. Before the AM adsorption on the cell edges was investigated, the supercell was again optimized, using the previously introduced setup (cell volume and shape were kept fixed).

3. Results and Discussion

To gain insight into the surface topology and AM adsorption properties of micro- and nanopores present in carbon derivatives such as hard carbon, graphitic model surfaces containing various types of defects such as MV, SW, MSW, and AA defects as well as impurities were examined.

Four primary categories were taken into consideration to investigate the adsorption of AM atoms on the graphitic surfaces: pristine graphite (G), defective graphite, defect-free graphite + impurities, and a combination of defects and impurities. The geometry optimization for each of the models under consideration was carried out using the parameters indicated in the computational methods section.

Mono-vacancies, created by removing a single carbon atom, belong to the most common defect types seen in graphitic materials. As a result, there are three undercoordinated carbon atoms that are triangularly arranged (see **Figure 1**b). The SW defect is a topological defect and is obtained via the so-called SW transformation (see Figure 1c). The latter one converts four carbon hexagons into two heptagons and two pentagons by rotating one C—C bond by 90°. Regarding the combination of MV and SW defects, it has to be mentioned that this combination creates a new form of defect with tetragonal, pentagonal, heptagonal, and decagonal units (see Figure 1d). Finally, an adatom, placed near a graphitic layer, preferentially adsorbs on a bridge site, forming two bonds with carbon atoms in the graphite plane (see Figure 1e).

To evaluate the respective adsorption processes on these surfaces, the resulting adsorption energies for defect- and impurity-containing systems were determined and compared with the

Research Article
doi.org/10.1002/batt.202500382
Chemistry Europe
European Chemical Societies Publishing

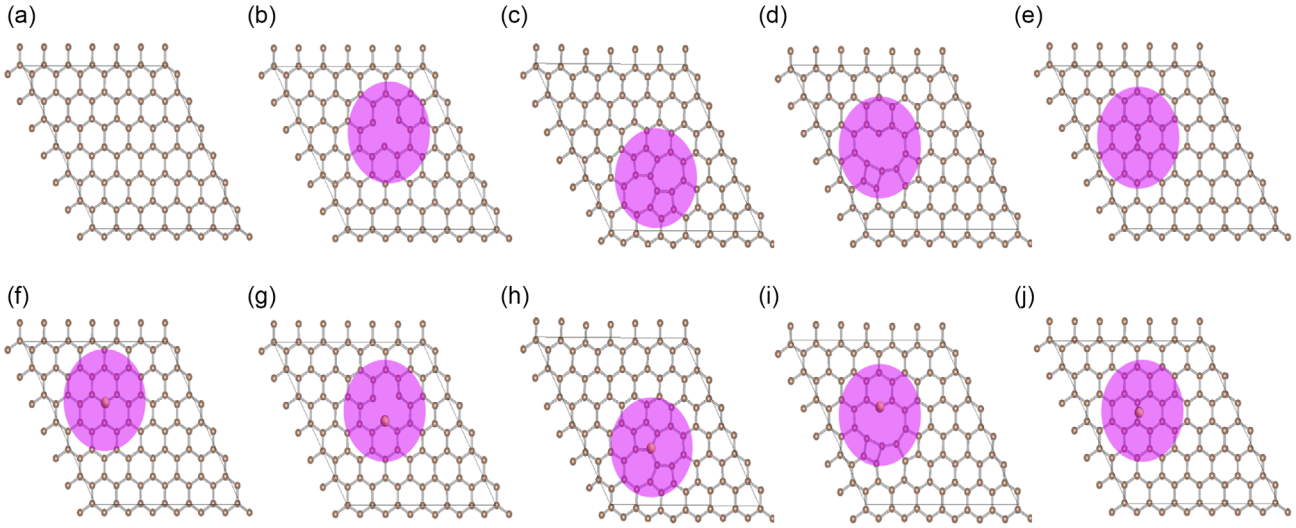

Figure 1. Top view of the different defect and impurity containing model surfaces that have been investigated. a) pristine graphite, b) MV defect, c) SW defect, d) MV + SW defect, e) adatom (carbon), f) pristine graphite + impurity, g) MV defect + impurity, h) SW defect + impurity, i) MV + SW defect + impurity, and j) adatom (impurity).

pristine graphite surface. The adsorption energy was computed via the following expression:

$$E_{ads} = E_{sys+AM} - (E_{sys} + E_{AM}) \quad (1)$$

where E_{sys+AM} represents the total energy of the graphitic surface including the defect or impurity as well as the adsorbed AM atom. E_{sys} corresponds to the energy of the considered surface model without adsorption. Finally, E_{AM} is the energy of the AM in the bulk metal phase.

3.1. Pristine and Defective Graphite

The adsorption energies for Li, Na, and K on pristine graphite amount to 0.19, 0.21, and −0.50 eV, respectively. Hence, Li and Na adsorption is not favorable on the pristine graphite surface with respect to the formation of bulk metal. The adsorption of K, on the other hand, is energetically favorable, which is in agreement with earlier studies.[37] To better understand this finding, the adsorbed AMs were investigated by analyzing the charge density differences with respect to the adsorption process. Indeed, the charge transferred from the K atom to the graphite surface is clearly higher and more spatially extended as compared to Li and Na (see **Figure 2**). This finding is also confirmed by the charge analysis using the DDEC6 method,[52,53] which yielded a charge transfer of 0.91 e for K, whereas for Li and Na lower values of 0.83 and 0.77 e were observed. This can be interpreted as a sign of the stronger K adsorption leading to a higher charge transfer.

For the case of the MV defect (see **Table 1** and **Figure 3**a–c), the AM atoms, originally placed above the center of the defect site, move toward one side of the triangle that surrounds the defect site. While the AM-free system is essentially undistorted,

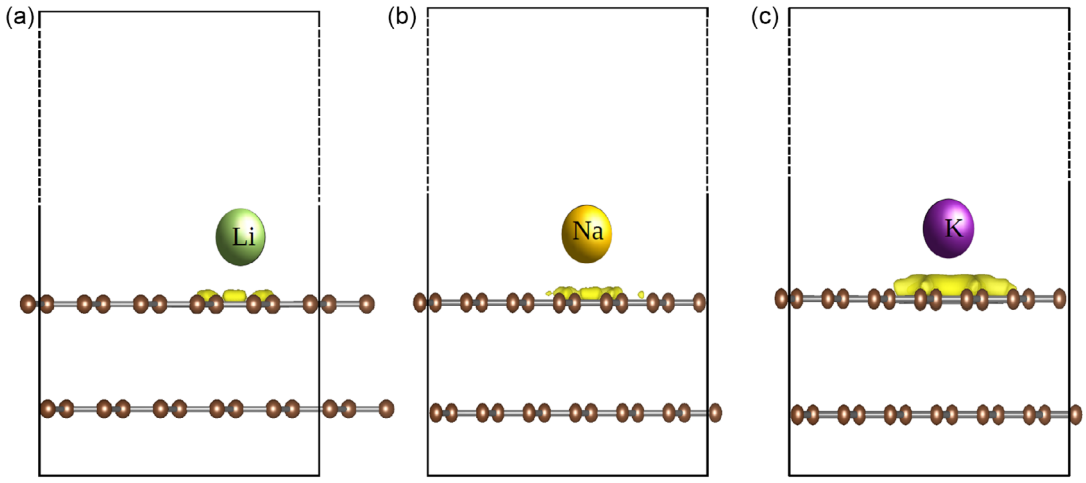

Figure 2. Charge density differences for a) Li, b) Na and c) K adsorption on pristine graphite (C_{144}). The yellow color shows the negative charge distribution for an isosurface value of 0.01 e Å^{-3}.

Research Article
doi.org/10.1002/batt.202500382
Chemistry Europe
European Chemical Societies Publishing

Table 1. Li, Na, and K adsorption energy E_{ads} (in eV) for the different types of defects and for pristine graphite (G).

Models	Li_1	Li_2	Li_3	Li_4	Na_1	Na_2	Na_3	Na_4	K_1	K_2	K_3	K_4
MV	−1.24	−0.33	−0.10	−0.21	−0.99	–	−0.07	–	−1.42	–	−0.80	–
SW	−0.1	0.03	0.14	−0.03	−0.04	0.08	0.18	0.06	−0.72	−0.65	−0.55	−0.70
MSW	−1.37	−0.36	−0.37	−0.08	−1.10	–	−0.37	−0.10	−1.52	–	–	−0.78
AA	−0.98	–	−0.10	–	−0.91	−0.89	−0.08	–	−1.47	−1.47	−0.83	–
G	0.19	–	–	–	0.21	–	–	–	−0.50	–	–	–

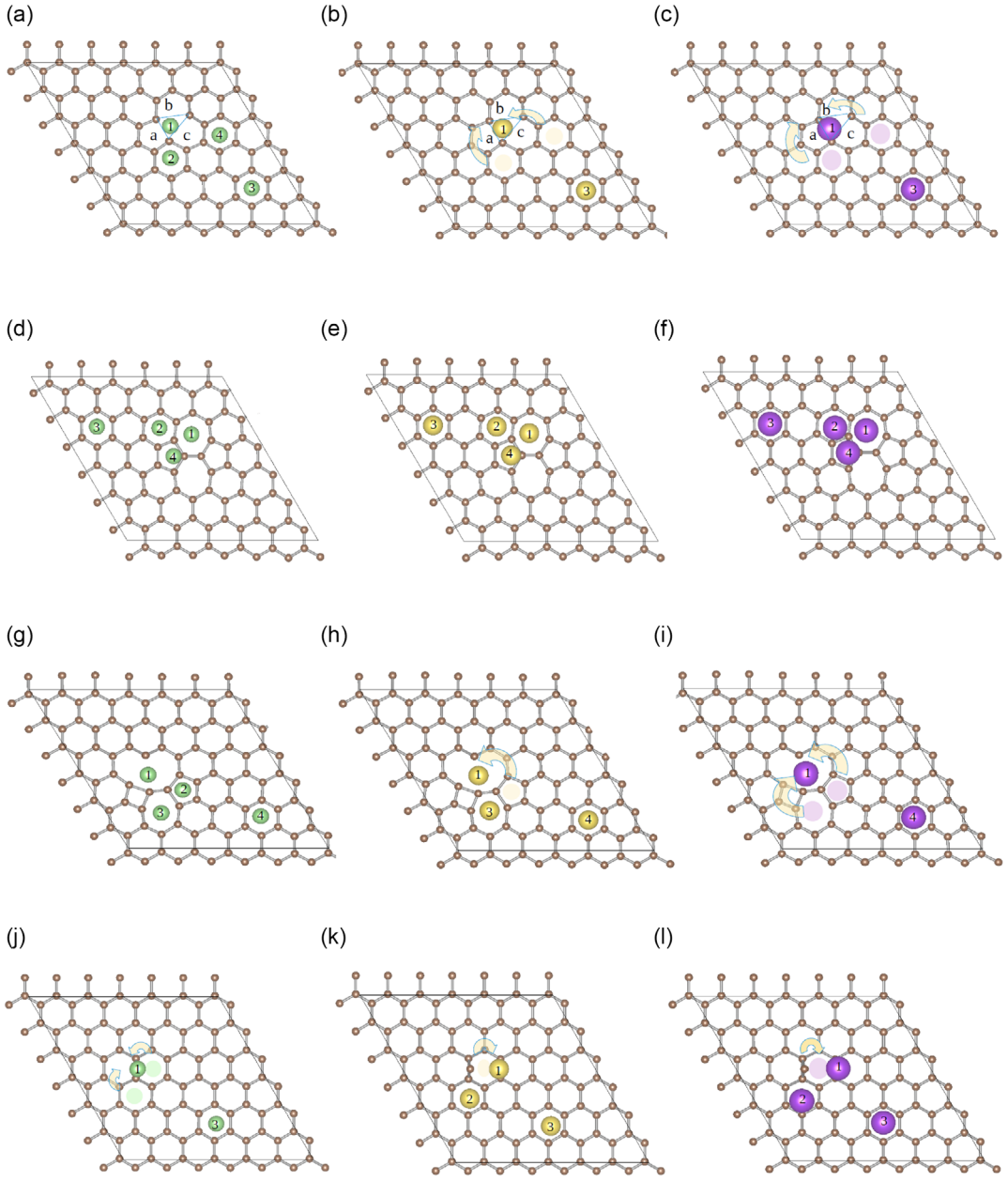

Figure 3. Possible Li, Na, and K-adsorption sites for the different model systems. Here only the top layer of the surface that contains the defect is shown. In a–c) the MV defect, in d–f) the SW defect, in g–i) the MSW defect and in j–l) the AA defect are depicted for Li (green), Na (yellow) and K (purple), respectively. Atoms that during relaxation have moved to a neighboring site are shown in faint color with an arrow indicating the site they have moved to.

the AM atom adsorption causes the corresponding carbon atoms to move out of the plane, thus resulting in the graphitic plane getting slightly curved (see Figure S11e, Supporting Information). The AM adsorption energy, in contrast, is significantly stabilized by the presence of the MV defect, such that Li (−1.24 eV), Na (−0.99 eV), and K (−1.42 eV) adsorption at the defect site become

energetically favorable, which for the case of Li and Na is in contrast to the defect-free system. For adsorption sites not directly neighboring the MV defect (see Figure 3a), Li is directly adsorbed at the center of the hexagon it is placed in. This scenario is also observed for Na and K atoms far from the defect site (see Figure 3b,c), whereas Na and K atoms placed in hexagons, neighboring the MV defect actually move to the defect center. In the case of surfaces containing SW defects (see Figure 3d–f), AM adsorption on four different sites is considered. Again, far from the defect site, the Li, Na, and K atoms adsorb in the hexagon centers. For the pentagon site (site number 4) the adsorption is slightly off-centered with the AM atoms moving toward the C-atom that is shared with the neighboring heptagons. For the hexagon site adjacent to a pentagon and a heptagon (site number 2) Li and Na essentially remain at the center of the hexagon, whereas the K atom moves slightly toward the C—C bond shared with the pentagon. Finally, AM atoms placed in the heptagon again prefer to stay almost centered with the system not showing considerable geometry change. As in the case of the MV defect, the presence of an SW defect also stabilizes the AM adsorption, however, to a much smaller extent (see Figure 3 and Table 1). This can be explained by the fact that the SW defect is only a structural transformation with all bonds remaining saturated, whereas the MV defect resulted in the creation of unsaturated dangling bonds. In general, if there is an even number of adjacent missing atoms, the graphite sheet can be completely recreated without dangling bonds. In contrast, if an odd number of neighboring atoms is missing, dangling bonds form on the graphite surface (see Figure S3, Supporting Information).[54] When the MSW defect is investigated, Li atoms are found to adsorb at the center of the different investigated sites, while the Na and K atoms from the pentagonal site move inside the decagon. The Na atoms placed on the heptagon and hexagon sites (far from the defect sites) remain in their positions as in the case of Li. This scenario is different for K, where atoms from the heptagon center also move inside the large decagon, which is likely to be due to the larger size of K. Finally, the K atoms on hexagonal sites far from the defect also remain essentially centered (see Figure 3i). For the case of MSW defects, the system slightly curves after the adsorption of the AM atoms. The AM adsorption energy for the most stable sites of the MSW defect becomes even more favorable than for isolated MV and SW defects. This is a consequence of the formation of the large decagon with under-coordinated C-atoms, which increases the driving force for AM adsorption (see Table 1). Finally, for the AA defect, Li atoms placed on a hexagonal site in the vicinity of the defect move to the top of the adatom (see Figure S8 and Table S5, Supporting Information). For Na and K, in contrast, the position on top of the defect is, compared to the site in the hexagon next to it, energetically less favorable (-0.82 and -1.18 eV for Na and K as compared to -0.91 and -1.47 eV on the hexagonal site). Na and K atoms that are placed in the hexagonal sites next to the adatom aim at increasing the distance to the latter one and move to the most distant bridge site of that hexagon (see site number 1 in Figure 3k,l). In all cases, AM atoms placed in hexagonal sites far from the AA remain in these hexagons with some slight off-centering, which can be understood as a consequence of the spatial extension of the AA defects. Despite the presence of the adatom, the underlying surface is not showing significant distortions. Eventually, like in the previous situations, the AM adsorption energies for the AA defect become considerably more favorable, as compared to the case of pristine graphite (see Figure 1).

With respect to the occurrence of such surface defects in potential anode materials, it has to be pointed out that the adsorption should not be too strong as this can result in the AM atoms being trapped at the corresponding site, hence causing capacity loss. A comparison of the results obtained for the different defects shows that the SW defect exhibits the most promising behavior with the adsorption energy of Na and Li on the defect site being only slightly negative. However, in addition to direct adsorption on the defect sites the impact of the defects on their environment is also of interest, confirming the well-known fact that defects are non-local,[55] meaning that they can influence the AM adsorption far from the defect sites (see Figure 3). This is also evident from the fact that at locations distant from the defect site slight differences in the C—C bond length are still observed ($\approx$0.01 Å). To further elaborate on this, the charge transfer during AM adsorption far from the defect was considered for the case of the MV defect. The DDEC6 charge analysis yields charges of 0.84, 0.91, and 0.85 e for Li, Na, and K at site number 3, respectively. This means that for Li and Na the charge transfer to the graphitic plain is increased as compared to pristine graphite, thus also explaining the observed stabilization of the adsorption further away from the defect (see Table 1). For the cases of AA, MV, and MSW defects, the adsorption energies for Li, Na, and K far from the defect center reach values of ≈ -0.1, ≈ -0.1, and ≈ -0.8 eV, hence making the adsorption, in comparison to the case of pristine graphite (Li 0.19 eV, Na 0.21 eV, and K -0.50 eV), energetically more favorable. The SW defect does not significantly influence the sites far from its location, meaning that the adsorption for Li and Na quickly becomes unfavorable again. Hence, a balance between the adsorption strength on the defect site and the extension of the defect would in principle be needed to tailor the best suited Li and Na adsorption properties.

3.2. Pristine Graphite + Impurities

Apart from defects, impurities are another way to manipulate the adsorption energy of AM atoms on graphitic surfaces. According to earlier studies impurities can effectively change the electronic structure of graphite, by functioning as electron donor or acceptor, consequently also affecting properties such as the adsorption energy.[56,57] The carbon atoms of pristine graphite show a sp2-hybridization, with σ bonds between the neighboring atoms of the hexagonal carbon rings. The remaining electrons are located in the unhybridized p-orbital, forming a conjugated π system. This situation is altered by doping and can result in a change in reactivity toward AM adsorption. Following this line of thought, different types of impurities such as B, Si, N, and S, with their valence electron numbers differing by -1, 0, $+1$, and $+2$ with respect to

Research Article
doi.org/10.1002/batt.202500382
Chemistry Europe
European Chemical Societies Publishing

carbon have been added to the considered graphitic model system (see Table S1 and Figure S4, Supporting Information). These impurities were introduced by replacing one C-atom in the graphite surface by the respective element. Furthermore, the impact of adding OH on top of the surface was investigated (see Figure S4 and S9, Supporting Information). Regarding the system geometry, it is interesting to note that while S and Si atoms move out of the plane, toward the underlying graphitic layer (see **Figure 4**a), for B and N-doping the layers stay flat, showing no significant deformation (as for the situation outlined in Figure 4b). Similar to the case of defects, introducing these impurities—N being the exception—strongly favors the adsorption for all the considered AM species, with the highest adsorption strength for the case of K.

When replacing a carbon atom with B, S, or Si, the hexagonal sites directly adjacent to the impurity are the most stable ones for AM adsorption. In the case of B-doping, the Li atoms in the next nearest hexagon, not containing the B impurity, remain centered, whereas the Na atoms shift in direction of the impurity (see Figure S4a–c, Supporting Information). K atoms in the vicinity of the defect, in contrast, migrate to the defect site, whereas Li, Na, or K atoms far from the defect site stay inside the hexagon they are placed in. When Si-doping is considered, the scenario is somewhat different. While Li atoms far from the impurity are again adsorbed on hexagonal sites, Li atoms placed next to the impurity site shift toward the impurity, thus taking an off-center position. Li atoms from the more distant hexagonal sites—the sites adjacent to the impurity-containing hexagon—shift toward the hexagon corner, thus approaching the Si impurity. For the case of Na and K, atoms, placed next to the impurity or even in the adjacent hexagon, move on top of the impurity (see Figure S4j–l, Supporting Information). Interestingly, Li only remains on top of the Si impurity when it is directly placed there, with this site being slightly less favorable (E_{ads} amounts to −0.36 eV as compared to −0.37 eV at the adjacent hexagonal site). Eventually, in the case of the S-doping, Li atoms remain on on-center positions for all hexagons, whereas Na and K atoms placed at the center of the defect containing hexagons move on top of the impurity. Here, the adsorption of Li on top of the impurity is again energetically slightly less favorable (by ≈0.02 eV). Na and K atoms located in hexagons adjacent to the defect shift to the hexagon corner approaching the C atom and the bridge site, respectively (see Figure S4g–i, Supporting Information). Finally, the atoms that are located far from the impurity site remain at the center of the hexagon they were originally placed in.

Overall, our results show that the presence of impurities can significantly alter the adsorption energy. Boron impurities behave as electron acceptors and therefore show the strongest impact on the adsorption strength, yielding adsorption energies of −0.98, −0.85, and −1.47 eV for Li, Na, and K at the impurity site, respectively (see **Table 2**). For Si impurities, which have the same number of valence electrons as the C atoms they are replacing, adsorption energies of −0.37, −0.35, and −1.03 eV are observed at the most stable sites, respectively (see Table 2). Here, the slight stabilization of the adsorption process is caused by the Si-introduced distortion of the graphite surface (see Figure 4c). When N doping is considered, in contrast to the above-discussed cases, adsorption of Li and Na remains unfavorable. Also for K, the energy gain is less pronounced than in the case of pristine graphite, however, adsorption remains energetically favorable (−0.38 eV). This is due to the fact that nitrogen does not significantly change the surface geometry but at the same time acts as electron donor, thus making the transfer of additional electrons from adsorbed AMs to the surface less favorable. Regarding the AM positions for the case of N impurities, Li atoms from the center of the hexagon shift to a bridge site of the impurity-containing hexagon, whereas Na and K atoms move to hexagonal sites

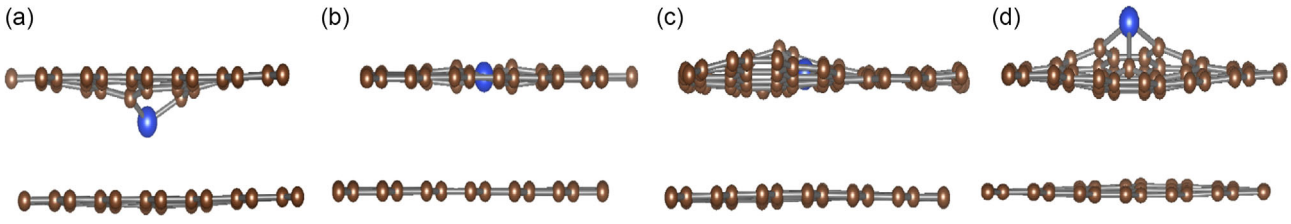

Figure 4. The different types of observed distortions fall into four categories that are depicted for the case of Si impurities. a) Impurity moving toward the layer below (as observed for pristine graphite + Si), b) slight distortion in the impurity-containing layer (as observed for MV + Si), c) strong distortion (bending) of the impurity containing layer (as observed for MSW + Si), and d) distortion (bending) of the impurity-containing layer with the impurity moving out of the plane (as observed for SW + Si). Additional information is provided in Figure S11, Supporting Information.

Table 2. Li, Na, and K adsorption energy E_{ads} (in eV) for the different types of impurities in pristine graphite.

Models	Li_1	Li_2	Li_3	Na_1	Na_2	Na_3	K_1	K_2	K_3
B	−0.98	−0.71	−0.44	−0.85	−0.65	−0.41	−1.47	−1.14	–
Si	−0.37	−0.04	0.08	−0.35	0.11	–	−1.03	−0.59	–
N	0.70	0.45	0.27	0.34	0.45	0.31	−0.36	−0.23	−0.39
S	−0.04	0.15	0.08	−0.10	0.15	0.13	−0.66	−0.55	−0.58

adjacent to the impurity-containing one. While the N—C bonds are slightly reduced (1.415 Å) as compared to the C—C bonds in pristine graphite (1.426 Å), this small variation does not significantly affect the geometry of the system. Eventually, S impurities result in a slight stabilization of the adsorption, amounting to −0.04, −0.10, and −0.66 eV for Li, Na, and K, respectively. This seems to be a consequence of the larger structural distortions introduced by S doping, which compensate for the fact that S in principle acts as an electron donor.

For an ideal anode material, the adsorption on the surface should be only slightly more stable as compared to the competing bulk metal phase. Hence, the observed trends for Si and S make these elements suitable candidates for modifying Li and Na adsorption. In contrast, the reduced adsorption strength observed for nitrogen doping make nitrogen impurities interesting candidates for K adsorption. To see if a further tuning of the AM adsorption strength is possible, additional elements from the same main group as nitrogen (X = P, As, Sb, Bi) have been investigated. However, due to the increasing atomic size, the C—X bonds are found to be elongated by 0.29, 0.48, 0.63, and 0.70 Å for P, As, Sb, and Bi, respectively. Obviously, this means that the surface geometry of the system is more significantly affected. In fact, the larger impurity atoms move out of the graphitic plane, thus resulting in curved graphitic sheets (similar to the scenario depicted in Figure 4d) and significantly increasing adsorption strength. While As, Sb, and Bi show a stronger adsorption with increasing dopant size for all AMs (see **Table** 2 and **3**), the situation for the P impurity is slightly different. Here, the AM atoms move from the doping site to the adjacent hexagon, which results in a significant increase in adsorption strength.

To summarize the impact of doping on the electronic structure, the Fermi energy shift for the different impurities is depicted with respect to the pristine graphitic system (see **Figure 5**). Boron and nitrogen doping result in the largest up/down shift of the Fermi level. This is a consequence of the essentially unaltered surface geometry and their role as electron acceptor/donor. The other investigated impurities introduce more severe surface distortions, which in the case of the considered electron donors (S, P, As, Sb, Bi) compensate for the additional valence electrons such that adsorption is strongly favored.

3.3. Combining Defects and Impurities

To further extend our study, the combination of defects (MV, SW, MSW) and impurities was investigated. This will be discussed for a few selected cases, whereas additional information for all considered combinations is provided in the SI. As previously discussed, for MV defects the AM atoms firmly bind to the defect site, which is a consequence of the dangling bonds and makes the defect site an ideal place for AM-atom adsorption. However, the fact that AM-atoms may be trapped in the defect site, is a drawback for battery applications causing capacity loss. While different approaches such as hydrogen saturation or structural healing of graphitic systems have been proposed to address problems resulting from structural defects,[58–63] here, we investigated a different pathway looking at the incorporation of various impurities and how they alter the reactivity in the vicinity of the defect sites. For combining an MV defect with an S impurity, one of the three carbon sites neighboring the defect site was replaced (see Figure S5 and Table S2, Supporting Information). In this case, the surface gets distorted and the system curves around the impurity site (similar to the situation depicted in Figure 4c), which is as a result of the bigger sulfur atoms as compared to carbon.[64] Consequently, this also results in an increased C—S bonds length of 1.74 Å whereas 1.42 Å are observed for undistorted C—C bonds. Our results furthermore show that S-doping weakens the adsorption strength on the defect site, resulting in adsorption energies of −0.53, −0.38, and −1.0 eV for Li, Na, and K, respectively (as compared to −1.24, −0.99, and −1.49 eV for the plain defect). Other impurities like Si and OH show similar but less pronounced effects, for instance −0.85 (−1.05), −0.69 (−0.88), and −1.24 eV (−1.19 eV) for Li, Na, and K adsorption on the defect sites for Si (OH) doping, respectively, as also depicted in **Figure 6**. Regarding the SW defect, one of the carbon atoms in the rotated bond was replaced by sulfur (see Figure S6 and Table S3, Supporting Information), resulting in larger distortions of the surface (similar to the scenario shown in Figure 4d). The three C—S bonds are not equal, with two of the C atoms shifting toward the underlying graphite layer, yielding a bond length of 1.78 Å. The remaining C atom shifts toward the vacuum, amounting to a C—S bond length of 1.68 Å. As in the previous case, the S-doping results in a beneficial modification of the surface, yielding adsorption energies of −0.45, −0.42, and −0.97 eV for Li, Na, and K, respectively. However, for the SW defect, N-doping also increases the adsorption strength for Li (−0.27 eV) and Na (−0.30 eV). In both

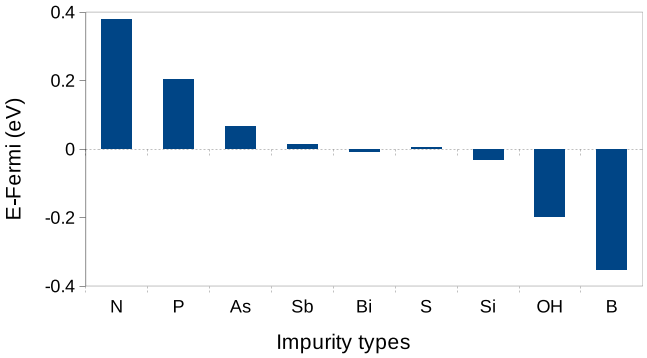

Figure 5. Fermi energy shift for the different types of impurities introduced in or added on top (OH) of pristine graphite. The shift in Fermi energy is calculated as $E_F(G + imp) - E_F(G)$.

Table 3. Adsorption energy E_{ads} (in eV) for Li, Na, and K atoms with respect to N, P, As, Sb, and Bi impurities in pristine graphite.

Models	Li	Na	K
N	0.70	0.34	−0.36
P	−0.77	−1.47	−1.51
As	−0.79	−0.75	−1.23
Sb	−1.32	−1.10	−1.50
Bi	−3.00	−2.51	−1.67

Research Article
doi.org/10.1002/batt.202500382
Chemistry Europe
European Chemical Societies Publishing

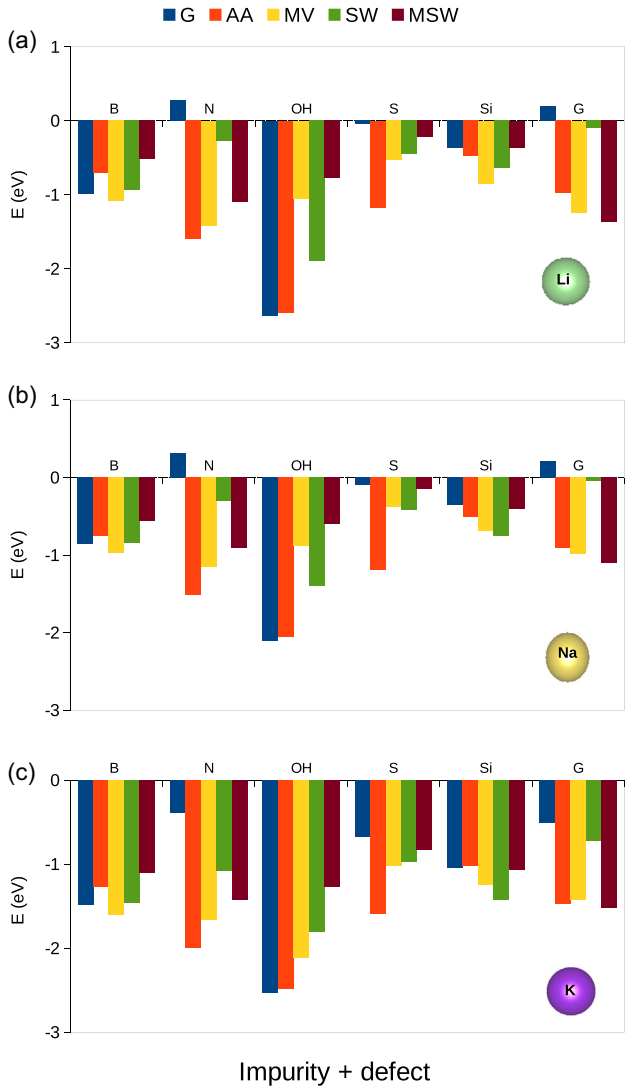

Figure 6. Adsorption energies for a) Li b) Na and c) K, for the combinations of different types of defects and impurities. The adsorption energies on pristine graphite (G) for Li, Na, and K are 0.19, 0.21, and −0.50 eV, respectively (without defects and impurities).

cases as compared to the impurity-free system, with Li and Na bonding energies of −0.1 and −0.04 eV, the change in adsorption energy is not so significant that a blocking of the AM-atoms has to be expected. It should be noted that OH, B, and S impurities highly increase the adsorption strength for Na, Li, and K, which indicates that these elements might be unfavorable for anode applications.

Finally, in case of the MSW defect, the twofold coordinated C atom in the decagon has been replaced by sulfur (see Figure S7 and Table S4, Supporting Information). For this scenario, the system shows distortions around the defect site (similar to the situation depicted in Figure 4c), which can be explained as result of the increasing C—S bond (1.73 Å) as compared to pristine graphite. As for the MV + S defect, for the MSW + S the adsorption energy of the AM atoms—amounting to −0.22, −0.13 and −0.83 eV for Li, Na and K—is significantly less negative as compared to the impurity-free model system (Li (−1.37 eV), Na (−1.10 eV), and K (−1.52 eV)).

When combining an MSW defect and an impurity, for all considered impurities, a decrease in adsorption strength is observed. This can be explained by the fact that the impurity atom replaces the carbon atom with the dangling bond, thus actually decreasing the reactivity of the system toward AM adsorption (see **Figure 7**a). Instead, when the impurity is placed at another site, the adsorption strength is increased. This has been studied for the case of boron, where replacing the carbon atom that is shared by the pentagon, the heptagon, and the decagon (see Figure 7b) shows that the adsorption strength increases for Li (−1.85 eV), Na (−1.54 eV), and K (−1.91 eV) as compared to the impurity-free system.

Hence, the combination of defects and impurities allows for further modification of the adsorption strength on graphitic surfaces. Due to lower adsorption strength, the combination of the N-doping with SW defects and also combining the MSW defect with S are of interest for Li and Na, while for the case of K, the combination of S-doping with the MSW defect is suited to alter the adsorption in the desired way.

3.4. Edge Defects and Curvature

In addition to impurities and planar defects, the edge sites of graphitic domains are also known to be potential AM adsorption sites. To investigate this point, additional calculations were performed (see Figure S10b, Supporting Information for the structure models used to represent edge sites and curved graphite). Our calculations confirm that AM atoms are strongly adsorbed at

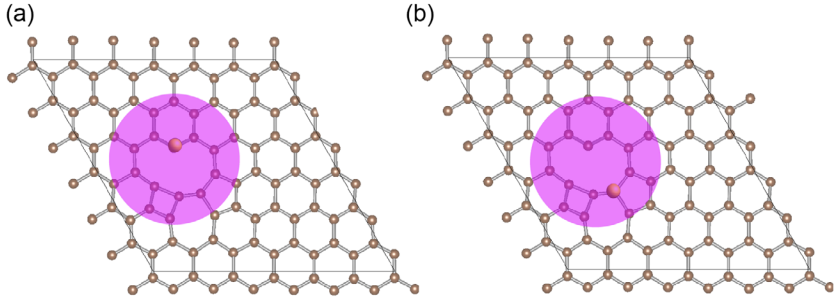

Figure 7. Impurity atom at two different sites of a MSW defect. a) On the site of the dangling bond and b) on the site shared by pentagon, heptagon, and decagon.

Research Article
doi.org/10.1002/batt.202500382
Chemistry Europe
European Chemical Societies Publishing

the edge sites, yielding adsorption energies of −3.01, −2.50, and −3.33 eV for Li, Na, and K, respectively. Due to the unsaturated bonds at the edge sites the adsorption energies are much stronger than on top of the pristine graphite surface. Hence, edge sites and related defects will result in extremely strong bonds, thus causing a significant capacity loss during the charge/discharge process. However, adding a single impurity to the edge site of the considered model highly alters the adsorption energy (more than 1.0 eV for Li, Na, and K), showing that impurities can also for this case act as a means for tailoring the adsorption properties. Notice that here only one carbon atom was replaced (by B, Si, and S), with the adsorption energy being obtained by adsorbing the AM atoms around the considered impurities. Hence, replacing additional carbon atoms at the edge sites with impurities may even be more beneficial, which is in agreement with earlier studies.[65,66]

Beside the just-discussed impurities, hydrogen saturation is also a straightforward technique to modify the adsorption properties of the edge sites, thus allowing for higher initial coulombic efficiency and efficient capacity retention.[59,67]

Finally, by inserting a large atom between the graphitic layers, we have introduced curvature into the graphitic domains. The structures were then optimized by keeping the bottom layer fixed, whereas the top layer was free to move and consequently curved around the intercalated atom. After removing the intercalant, we considered two selected sites for AM atom adsorption on the obtained, curved surface (see Figure S10a, Supporting Information). The adsorption of Li and Na on negatively (syncline) and positively (anticline) curved sites are slightly more favorable as for pristine graphite (by about 0.1 eV). For the case of K, the adsorption on the positively curved sites does not show a considerable change compared to the pristine graphite surface. K adsorption on the negatively curved site, in contrast, is favorable by more than 0.1 eV. This can be understood as a consequence of the size of the K atom and its therefore extended interaction with the graphite surface which makes K adsorption more stable on negatively curved sites. This is due to negatively curved site providing more surface area for the interaction of K with graphite as compared to positively curved site.

Thus, while AM atoms strongly bind to edge sites, impurities and/or bond saturation can largely reduce the potential capacity loss. Furthermore, introducing curvature—e.g., by applying stress to the material—may also be a way to alter the adsorption properties, in particular to enhance the Li and Na adsorption.

3.5. Diffusion Barriers

To investigate the impact of different structural changes on the AM kinetics of the graphitic model systems, the NEB approach was applied. A few cases, including B and S impurities as well as SW and MV defects (see **Figure 8**), were selected to quantify the energy barriers for the AM diffusion near the defect and impurity sites. Moreover, the results for pristine graphite, MSW defect, and N-doped graphite are depicted in Figure S11, Supporting Information. To estimate the diffusion barriers, the minimum energy path of AM atoms, diffusing from the most stable site in the vicinity of the defect to a neighboring hexagonal site, were determined. The ion mobility is one of the crucial performance parameters for an electrode material as it determines the charge/discharge rates as well as loss of active material due to ion trapping. Hence, low diffusion barriers are highly desirable. Before discussing defect and impurity containing scenarios, AM diffusion from the center of one hexagon to that of an adjacent one have been considered for a pristine graphite surface. The resulting diffusion barriers amount to 0.25, 0.05, and 0.04 eV for Li, Na, and K, respectively (see Figure S12, Supporting Information), indicating fast surface diffusion, especially for Na and K. For the case of a boron impurity, the activation energy for Li, Na, and K diffusion amount to 0.40, 0.22, and 0.12 eV, respectively, meaning that Li is facing a higher barrier to diffuse away from the defect site. Here, it has to be noted that for the case of K, the adjacent hexagonal site does not correspond to a local minimum. To allow for comparison with Li and Na, the K atom was fixed on the hexagonal site and only optimized in *z*-direction. When S-doping is considered, the barriers that Li, Na, and K atoms have to overcome to move away from the defect amount to 0.33, 0.27, and 0.14 eV, respectively. Compared to B-doping, S-doping shows a lower activation barrier, especially for Li and Na, hence pointing to an improved ion mobility in the presence of sulfur. Finally, the AM diffusion in the presence of SW, MV, and MSW defects was investigated. For the MV defect, Li, Na, and K have to overcome increased barriers of 0.88, 0.52, and 0.37 eV, respectively, for leaving the defect site and moving to a neighboring hexagonal site. For this scenario, it has again to be noted that the neighboring hexagonal sites are no local minima for Na and K. Hence, to allow for an estimate of the diffusion barrier, as for the boron impurity, Na and K atoms were fixed on a hexagon, optimizing the final state of the diffusion path only along the *z*-direction. For the MSW defect similar results are

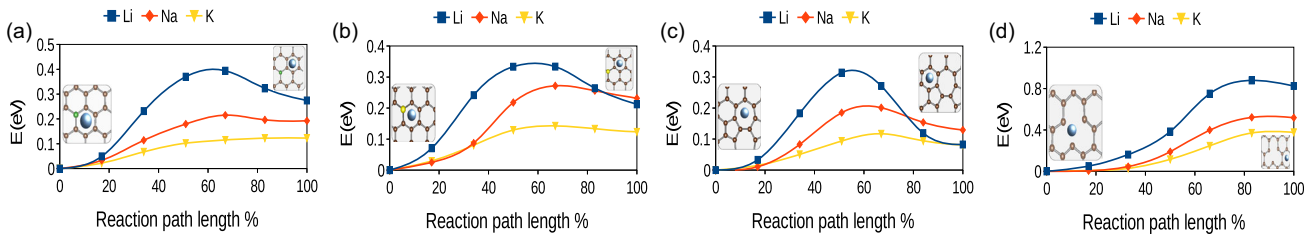

Figure 8. Diffusion barriers for AM atom migration from neighboring site (hexagon) to defect site (hexagon) for a) B doping, b) S doping, c) SW defect, and d) MV defect.

obtained (see Figure S12, Supporting Information). Eventually, when the SW defect is considered, the AM atoms face barriers of 0.31, 0.2, and 0.11 eV for Li, Na, and K, respectively, to move from the decagon site to the neighboring hexagon.

While the different impurities and defect types largely affect the diffusion barriers, a faster diffusion of K ions is observed for all cases.

The fact that a large part of the diffusion barrier is due to the difference in energy between the initial and final states means that the diffusion away from defect/impurity sites is dominated by the adsorption energy on these sites. Moreover, the diffusion barriers on pristine graphite are almost zero for Na and K, meaning that these AMs can basically diffuse freely as soon as they have left the defect site. Hence, the incorporation of S impurity and SW defects seems well suited for Li and Na adsorption and diffusion, since they overcome the instability with respect to adsorption without blocking/trapping the AM atoms during the charge/discharge process.

4. Conclusion

In this work, the AM adsorption energies on graphite based surfaces in the presence of defects and impurities have been determined via first-principles calculations, thus allowing to assess the corresponding changes in adsorption strength as compared to a pristine graphite surface. Here, it has to be pointed out that an ideal anode material should also be able to store/adsorb AMs on the surface. For pristine graphite, this is only fulfilled for the case of K, whereas Li and Na actually do not stably adsorb, thus calling for surface modifications. However, the adsorption strength should at the same time not be too high, since this can result in trapped AM atoms at the defect/impurity sites. Our results show that both defects and impurities can significantly increase the adsorption strength, which is a consequence of structural distortions and changes in the electronic structure. While defect types like MV, MSW, and AA result in strong bonds with the adsorbate, SW defects result in the desired slight stabilization of the Li and Na adsorption. For impurities, the same considerations are valid and S-doping is found to result in the stabilization of Li and Na adsorption. N-doping, in contrast, can be considered the best option for decreasing the adsorption strength for K. In summary we find that the combination of defects with in particular Si and S impurities can help to optimize the adsorption strength for Li and Na in carbon based anodes with large surface areas such as hard carbon. In contrast, defect free N-doped surfaces provide the best adsorption properties for the case of K. Furthermore, we observed that the diffusion kinetics in the vicinity of defects and impurities is largely determined by the energy difference between the initial and final states, such that the adsorption strength is also the limiting factor for diffusion. This means that S and Si impurities in combination with defects are again well-suited candidates for Li and Na.

In general, our results indicate that designing carbon based anode materials with particular defects and impurities may provide improved electrodes which are of particular importance in modern energy storage technologies. Here, further insights for increased system sizes and more complex surface structures are necessary and may, for instance, be obtained by extending our findings using machine learning derived force fields.

Supporting Information

Additional results and figures are given in Supporting Information file (SI).

Acknowledgements

This work was supported by the Cluster of Excellence EXC 2154 "Post-Li Storage", project ID 390874152, funded by the German Research Foundation (DFG). The authors acknowledge support by the state of Baden-Württemberg through bwHPC and the DFG through grant no INST 40/575-1 FUGG (JUSTUS 2 cluster) and by the HoreKa supercomputer funded by the Ministry of Science, Research and the Arts Baden-Württemberg, and by the Federal Ministry of Education and Research. This work contributes to the research performed at CELEST (Center for Electrochemical Energy Storage Ulm-Karlsruhe).

Open Access funding enabled and organized by Projekt DEAL.

Conflict of Interest

The authors declare no conflict of interest.

Data Availability Statement

The data that support the findings of this study are available from the corresponding author upon reasonable request.

Keywords: adsorption · defects and impurities · graphite · post-Li ion batteries

[1] M. Li, J. Lu, Z. Chen, K. Amine, *Adv. Mater.* **2018**, *30*, 1800561.
[2] M. Wakihara, *Mater. Sci. Eng.: R: Rep.* **2001**, *33*, 109.
[3] T. Kim, W. Song, D.-Y. Son, L. K. Ono, Y. Qi, *J. Mater. Chem. A* **2019**, *7*, 2942.
[4] W. Van Schalkwijk, B. Scrosati, *Advances in Lithium-Ion Batteries*, Springer, New York, NY **2002**, pp. 1–5.
[5] M. D. Slater, D. Kim, E. Lee, C. S. Johnson*Adv. Funct. Mater.* **2013**, *23*, 947.
[6] J.-Y. Hwang, S.-T. Myung, Y.-K. Sun, *Chem. Soc. Rev.* **2017**, *46*, 3529.
[7] R. Rajagopalan, Y. Tang, X. Ji, C. Jia, H. Wang, *Adv. Funct. Mater.* **2020**, *30*, 1909486.
[8] X. Min, J. Xiao, M. Fang, W. A. Wang, Y. Zhao, Y. Liu, A. M. Abdelkader, K. Xi, R. V. Kumar, Z. Huang, *Energy Environ. Sci.* **2021**, *14*, 2186.
[9] Y. Wen, K. He, Y. Zhu, F. Han, Y. Xu, I. Matsuda, Y. Ishii, J. Cumings, C. Wang, *Nat. Commun.* **2014**, *5*, 4033.
[10] Z.-L. Xu, G. Yoon, K.-Y. Park, H. Park, O. Tamwattana, S. J. Kim, W. M. Seong, K. Kang, *Nat. Commun.* **2019**, *10*, 2598.
[11] G. Yoon, H. Kim, I. Park, K. Kang, *Adv. Energy Mater.* **2017**, *7*, 1601519.
[12] Y. Okamoto, *J. Phys. Chem. C* **2014**, *118*, 16.
[13] J. Langer, V. Epp, P. Heitjans, F.-A. Mautner, M. Wilkening, *Phys. Rev. B: Condens. Matter Mater. Phys.* **2013**, *88*, 094304.
[14] L. Liang, M. Tang, Q. Zhu, W. Wei, S. Wang, J. Wang, J. Chen, D. Yu, H. Wang, *Adv. Energy Mater.* **2023**, *13*, 2300453.

[15] M. Zhang, Y. Li, F. Wu, Y. Bai, C. Wu, *Nano Energy* **2021**, *82*, 105738.
[16] Z. Li, Y. Chen, Z. Jian, H. Jiang, J. J. Razink, W. F. Stickle, J. C. Neuefeind, X. Ji, *Chem. Mater.* **2018**, *30*, 4536.
[17] L. Xie, C. Tang, Z. Bi, M. Song, Y. Fan, C. Yan, X. Li, F. Su, Q. Zhang, C. Chen, *Adv. Energy Mater.* **2021**, *11*, 2101650.
[18] J. F. Peters, M. Abdelbaky, M. Baumann, M. Weil, *Matér. Tech.* **2019**, *107*, 503.
[19] D.-Y. Kim, D.-H. Kim, S.-H. Kim, E.-K. Lee, S.-K. Park, J.-W. Lee, Y.-S. Yun, S.-Y. Choi, J. Kang, *Nanomaterials* **2019**, *9*, 793.
[20] H.-J. Kang, Y. S. Huh, W. B. Im, Y.-S. Jun, *ACS Nano* **2019**, *13*, 11935.
[21] M. Thompson, Q. Xia, Z. Hu, X. S. Zhao, *Mater. Adv.* **2021**, *2*, 5881.
[22] K.-. Hong, L. Qie, R. Zeng, Z.-q. Yi, W. Zhang, D. Wang, W. Yin, C. Wu, Q.-j. Fan, W.-x. Zhang, Y.-h. Huang, *J. Mater. Chem. A* **2014**, *2*, 12733.
[23] P. Liu, Y. Li, Y.-S. Hu, H. Li, L. Chen, X. Huang, *J. Mater. Chem. A* **2016**, *4*, 13046.
[24] A. Beda, J.-M. L. Meins, P.-L. Taberna, P. Simon, C. M. Ghimbeu, *Sustainable Mater. Technol.* **2020**, *26*, e00227.
[25] E. Irisarri, A. Ponrouch, M. Palacin, *J. Electrochem. Soc.* **2015**, *162*, A2476.
[26] S.-Y. Long, J.-L. Liu, X.-Q. Xian, L.-Q. Zhou, W.-D. Lv, P.-D. Tang, Q.-S. Du, *Sci Rep.* **2023**, *13*, 23063.
[27] Z. Sun, X. Shi, X. Wang, Y. Sun, *Diam. Relat. Mater.* **1999**, *8*, 1107.
[28] C. Cai, Y. Chen, P. Hu, T. Zhu, X. Li, Q. Yu, L. Zhou, X. Yang, L. Mai, *Small* **2022**, *18*, 2105303.
[29] I. Zsoldos, *Nanotechnology, Science and Applications* **2010**, DovePress; pp. 101–106.
[30] R. P. Hardikar, D. Das, S. S. Han, K.-R. Lee, A. K. Singh, *Phys. Chem. Chem. Phys.* **2014**, *16*, 16502.
[31] Y. Tian, H. Yang, Y. Zeng, Y. Qi, W. Wang, H. Chen, W. Yin, Y. Ke, Z. Jian, W. H. Kan, W. Chen, *Acs Appl. Energy Mater.* **2023**, *6*, 3854.
[32] B. Liu, P. Huang, M. Liu, Z. Xie, *J. Mater. Sci.* **2021**, *56*, 17682.
[33] C. M. Ghimbeu, J. Górka, V. Simone, L. Simonin, S. Martinet, C. Vix-Guterl, *Nano Energy* **2018**, *44*, 327.
[34] A. Kumar, P. Raizada, A. Hosseini-Bandegharaei, V. K. Thakur, V.-H. Nguyen, P. Singh, *J. Mater. Chem. A* **2021**, *9*, 111.
[35] H. Lan, L. Li, X. An, F. Liu, C. Chen, H. Liu, J. Qu, *Appl. Catal. B: Environ.* **2017**, *204*, 49.
[36] E. Olsson, G. Chai, M. Dove, Q. Cai, *Nanoscale* **2019**, *11*, 5274.
[37] H. Yildirim, A. Kinaci, Z.-J. Zhao, M. K. Chan, J. P. Greeley, *ACS Appl. Mater. Interfaces* **2014**, *6*, 21141.
[38] B. Lee, M. Kim, S. Kim, J. Nanda, S. J. Kwon, H. D. Jang, D. Mitlin, S. W. Lee, *Adv. Energy Mater.* **2020**, *10*, 1903280.
[39] K. Rytkönen, J. Akola, M. Manninen, *Phys. Rev. B* **2007**, *75*, 075401.
[40] Z. Li, C. Bommier, Z. S. Chong, Z. Jian, T. W. Surta, X. Wang, Z. Xing, J. C. Neuefeind, W. F. Stickle, M. Dolgos, P. A. Greaney, X. Ji, *Adv. Energy Mater.* **2017**, *7*, 1602894.
[41] R. Morita, K. Gotoh, M. Fukunishi, K. Kubota, S. Komaba, N. Nishimura, T. Yumura, K. Deguchi, S. Ohki, T. Shimizu, H. Ishidaa, *J. Mater. Chem. A* **2016**, *4*, 13183.
[42] S. Alvin, H. S. Cahyadi, J. Hwang, W. Chang, S. K. Kwak, J. Kim, *Adv. Energy Mater.* **2020**, *10*, 2000283.
[43] H. Euchner, B. P. Vinayan, M. A. Reddy, M. Fichtner, A. Groß, *J. Mater. Chem. A* **2020**, *8*, 14205.
[44] M. A. Reddy, M. Helen, A. Groß, M. Fichtner, H. Euchner, *ACS Energy Lett.* **2018**, *3*, 2851.
[45] J. Azizi, A. Groß, H. Euchner, *ChemSusChem* **2024**, *17*, e202301493.
[46] J. Azizi, A. Groß, H. Euchner, *ACS Appl. Mater. Interfaces* **2025**. *17*, 33965.
[47] H. S. Nguyen, A. Latz, *Phys. Chem. Chem. Phys.* **2023**, *25*, 28196.
[48] G. Kresse, J. Furthmüller, *Phys. Rev. B* **1996**, *54*, 11169.
[49] G. Kresse, D. Joubert, *Phys. Rev. B* **1999**, *59*, 1758.
[50] G. Henkelman, H. Jónsson, *J. Chem. Phys.* **1999**, *111*, 7010.
[51] G. Henkelman, H. Jónsson, *J. Chem. Phys. 113*, **2000**, 9978.
[52] T. A. Manz, N. G. Limas, *RSC Adv.* **2016**, *6*, 47771.
[53] N. G. Limas, T. A. Manz, *RSC Adv.* **2016**, *6*, 45727.
[54] M. D. Bhatt, H. Kim, G. Kim, *RSC Adv.* **2022**, *12*, 21520.
[55] D. Escaff, *Eur. Phys. J. D* **2011**, *62*, 33.
[56] D. H. Gharib, S. Gietman, F. Malherbe, S. E. Moulton, *Carbon* **2017**, *123*, 695.
[57] N. Tsubouchi, S. Shikata, *Nucl. Instrum. Methods Phys. Res., Sect. B* **2012**, *286*, 303.
[58] J. Jiao, H. Lu, C. Yi, D. Yang, X. Zeng, J. Lin, H. Li, *Chem. Eng. J.* **2024**, *500*, 156878.
[59] W. Li, M. Zhao, X. Zhao, Y. Xia, Y. Mu, *Phys. Chem. Chem. Phys.* **2010**, *12*, 13699.
[60] J. Chen, T. Shi, T. Cai, T. Xu, L. Sun, X. Wu, D. Yu, *Appl. Phys. Lett.* **2013**, *102*, 103107.
[61] W. Möller, B. Scherzer, *Appl. Phys. Lett.* **1987**, *50*, 1870.
[62] C. Lechner, P. Baranek, H. Vach, *Carbon* **2018**, *127*, 437.
[63] I. N. Kholmanov, J. Edgeworth, E. Cavaliere, L. Gavioli, C. Magnuson, R. S. Ruoff, *Adv. Mater.* **2011**, *23*, 1675.
[64] J. C. Slater, *J. Chem. Phys.* **1964**, *41*, 3199.
[65] J. Nie, S. Sun, Y. Song, B. Lu, A. Soh, J. Zhang, *J. Energy Storage* **2022**, *47*, 103568.
[66] K. Zhu, D. Kramer, C. Peng, *J. Energy Chem.* **2024**, *90*, 337.
[67] M. Wang, C. M. Li, *Nanoscale* **2011**, *3*, 2324.

Manuscript received: May 17, 2025
Revised manuscript received: July 29, 2025
Version of record online: